

LETTER TO THE EDITOR

# Spatially resolving the AGB star V3 in the metal-poor globular cluster 47 Tuc with VLT/GRAVITY <sup>★</sup>

K. Ohnaka<sup>1</sup>, G. Weigelt<sup>2</sup>, K.-H. Hofmann<sup>2</sup>, and D. Schertl<sup>2</sup>

<sup>1</sup> Instituto de Astrofísica, Departamento de Ciencias Físicas, Facultad de Ciencias Exactas, Universidad Andrés Bello, Fernández Concha 700, Las Condes, Santiago, Chile  
e-mail: k1.ohnaka@gmail.com

<sup>2</sup> Max-Planck-Institut für Radioastronomie, Auf dem Hügel 69, 53121 Bonn, Germany

Received / Accepted

## ABSTRACT

*Context.* Mass loss at the asymptotic giant branch (AGB) plays an important role not only in the final fates of stars, but also in the chemical evolution of galaxies. Nevertheless, the metallicity effects on AGB mass loss are not yet fully understood.

*Aims.* We present spatially resolved observations of an AGB star, V3, in the metal-poor globular cluster 47 Tuc (NGC 104).

*Methods.* The AGB star 47 Tuc V3 was observed using the GRAVITY instrument at ESO's Very Large Telescope Interferometer (VLT) at 2–2.45  $\mu\text{m}$ , with a projected baseline length of up to 96 m.

*Results.* The object 47 Tuc V3 has been spatially resolved and stands as the first to attempt to spatially resolve an individual star in a globular cluster. The uniform-disk fit to the observed data results in an angular diameter of  $\sim 0.7$  mas. Our modeling of the spectral energy distribution and near-infrared interferometric GRAVITY data suggests that the observed data can be explained by an optically thin dust shell with a 0.55  $\mu\text{m}$  optical depth of 0.05–0.25, consisting of metallic iron grains, likely together with effects of the extended atmosphere of the central star. The dust temperature at the inner shell boundary is 500–800 K (corresponding to 23–90 stellar radii), significantly lower than observed in nearby oxygen-rich AGB stars. Radiation pressure on small ( $< 0.05 \mu\text{m}$ ) iron grains is not sufficient to drive stellar winds. Therefore, iron grains may grow to larger sizes, even in the metal-poor environment. Alternatively, it is possible that the observed iron grain formation is a result of the mass outflow initiated by some other mechanism(s).

*Conclusions.* The sensitivity and angular resolution of VLT provides a new window onto spatially resolving individual stars in metal-poor globular clusters. This allows us to improve subsequent studies of the metallicity dependence of dust formation and mass loss.

**Key words.** infrared: stars – techniques: interferometric – stars: mass-loss – stars: AGB and post-AGB – (Stars:) circumstellar matter (Galaxy:) globular clusters: individual: 47 Tuc (NGC 104)

## 1. Introduction

Low- and intermediate-mass stars experience significant mass loss at the asymptotic giant branch (AGB), which plays an important role not only in stellar evolution, but also in the chemical evolution of galaxies. To incorporate the mass loss in the stellar evolution theory, we need a mass-loss formula, which expresses the mass-loss rate as a function of basic stellar parameters, such as the stellar mass, luminosity, temperature, and metallicity. However, the observationally derived mass-loss formulae show noticeable differences due to our incomplete understanding of the mass-loss mechanism (e.g., Vassiliadis & Wood 1993; van Loon et al. 2005; Goldman et al. 2017).

To improve our understanding of the metallicity dependence of mass loss, access to observations of stars with different metallicities are crucial. In this context, AGB stars in metal-poor globular clusters in the Milky Way provide us with excellent opportunities to work toward this goal. Furthermore, because the distance to globular clusters is often well known, the luminosity of each star can be determined. 47 Tuc (NGC 104) is one of the best

studied globular clusters at a distance of 4.5 kpc (Harris 1996<sup>1</sup>). Its low metallicity of  $[\text{Fe}/\text{H}] = -0.72$  (Harris 1996) is  $\sim 1/5$  the solar value, making it ideal for studying the AGB mass loss at low metallicities. McDonald et al. (2019) analyzed the radio CO observations of the pulsating AGB star V3 in 47 Tuc and found that the terminal velocity is slower than its Galactic counterparts. This study suggested that the lower metallicity results in smaller grains, which, in turn, slow down the stellar wind.

Dust is expected to form at lower temperatures in more metal-poor environments. The modeling of the observed spectral energy distributions (SEDs) of dusty AGB stars in the metal-poor globular clusters 47 Tuc and NGC 362 ( $[\text{Fe}/\text{H}] = -1.16$ ) shows that the dust condensation temperature is 600–1100 K (McDonald et al. 2011a, hereafter Mc11a; Boyer et al. 2009). These temperatures are much lower than the dust condensation temperature of  $\sim 1500$  K observed in the Galactic oxygen-rich AGB stars. However, there are ambiguities in the SED fitting, owing to the degeneracy coming from many parameters such as the dust condensation radius, density distribution, grain species, and grain size. A straightforward approach to mitigate this degeneracy and better constrain the metallicity effects is to spatially resolve the circumstellar dust envelope.

Send offprint requests to: K. Ohnaka

<sup>★</sup> Based on observations made with ESO's VLT/GRAVITY. Program ID: 112.25EN.001

<sup>1</sup> <https://physics.mcmaster.ca/~harris/mwgc.dat>

## 2. Observations and data reduction

The star V3 is one of the brightest AGB stars in the near-infrared in 47 Tuc. Its variability with a period of 192 days and amplitude of  $\Delta V \approx 5$  mag, along with the line doubling that is due to stellar pulsation, indicate that it is a Mira-like variable (Lebzelter et al. 2005). We observed 47 Tuc V3 with GRAVITY (GRAVITY Collaboration 2017) at ESO’s Very Large Telescope Interferometer (VLTI) on 2023 October 14 (UTC) at 2–2.45  $\mu\text{m}$ , using the Auxiliary Telescope (AT) configuration D0-G2-K0-J3, with a maximum projected baseline length of  $\sim 96$  m (Program ID: 112.25EN.001, P.I.: K. Ohnaka). HD3689 (F6V, uniform-disk diameter = 0.236 mas, JMMC catalog: Bourges et al. 2017) and HR9106 (F5V, uniform-disk diameter = 0.226 mas) were observed for the interferometric and spectroscopic calibration. However, the GRAVITY data of HR9106 show that it is spatially resolved, although it is expected to be a point source, according to its angular diameter from the JMMC catalog. Therefore, we only used HD3689 for the calibration of 47 Tuc V3. Our GRAVITY observations are summarized in Table A.1.

The GRAVITY data were reduced with the GRAVITY pipeline ver 1.6.0<sup>2</sup>. The data were originally taken with a spectral resolution of 500. To increase the signal-to-noise ratio (S/N) of the results, we spectrally binned the raw GRAVITY data (both the science target and the calibrator as well as the raw calibration files needed to create the P2VM) with a running box car filter, which resulted in a spectral resolution of 200. Each data set of the science target or calibrator consists of two exposures on the target and one on the sky. We reduced each exposure separately and then averaged the visibilities obtained from two exposures. The errors in the calibrated visibilities of V3 were computed from the errors given by the pipeline and the variations in the transfer function calculated from three data sets of HD3689. The spectroscopic calibration was carried out as described in Appendix B.

## 3. Results

Figure 1a shows the observed visibilities of V3 as a function of spatial frequency. The visibilities obtained at the longest baselines of 85–96 m (spatial frequencies of 180–220  $\text{arcsec}^{-1}$ ) are  $\sim 0.97$ , lower than 1 expected for a point source. The data points at a spatial frequency of  $\sim 150$   $\text{arcsec}^{-1}$  are also systematically slightly below 1, suggesting that the object is marginally resolved at a baseline length of  $\sim 70$  m. This is the first spatially resolved observation of an individual star in a globular cluster. The differential phases and closure phases are zero within measurement errors of  $\sim 1^\circ$ .

We fitted the visibilities observed at each wavelength with a Gaussian and a uniform disk (UD). The resulting FWHM and UD diameter, shown in Fig. 1b, are  $\sim 0.4$  mas and  $\sim 0.65$  mas, respectively, between 2.1 and 2.3  $\mu\text{m}$ . The UD diameter of the central star is estimated to be 0.38 mas from a stellar photospheric radius of  $185 R_\odot$  (Sect. 4) and the distance of 4.5 kpc. The visibilities expected from the uniform disks with the diameters of 0.65 and 0.38 mas are also shown in Fig. 1b. The measured UD diameter of  $\sim 0.65$  mas is 1.7 times larger than that of the central star. This may be interpreted as evidence of an extended dust envelope.

However, we suggest that a different interpretation is also plausible. The linear radius derived from the luminosity and effective temperature (see Sect. 4) corresponds to the photospheric radius. The apparent diameter of Mira stars can be

larger than the photospheric diameter due to their extended atmospheres. Woodruff et al. (2008, 2009) and Wittkowski et al. (2008) showed that the angular diameter of Mira stars reaches a minimum at 1.2–1.4  $\mu\text{m}$ , which approximately corresponds to the photospheric diameter, while the uniform-disk diameter at 2.2  $\mu\text{m}$  can be larger than that at 1.2–1.4  $\mu\text{m}$  by a factor of up to  $\sim 1.4$ . The UD diameter of 0.65 mas measured at 2.2  $\mu\text{m}$  is 1.7 times larger than the photospheric size of 0.38 mas – greater than the aforementioned factor of 1.4. However, if we adopt  $T_{\text{eff}} = 2900$  K instead of 3200 K in the calculation of the photospheric radius (Sect. 4), the stellar angular diameter is 0.46 mas and the measured 2.2  $\mu\text{m}$  UD diameter is 1.4 times larger than the photospheric size, as expected from the aforementioned studies. This means that the observed visibilities can also be interpreted as due to the extended atmosphere of V3 with none or just a slight contribution from a dust shell at 2–2.45  $\mu\text{m}$ . It is possible that the data are explained by the contributions of both the dust envelope and the extended atmosphere.

The obtained FWHM and UD diameter tend to increase shortward of 2.1  $\mu\text{m}$  and longward of  $\sim 2.3$   $\mu\text{m}$ . This can be explained as follows. The flux contribution of the central star is lower at  $\lesssim 2.1$   $\mu\text{m}$  and  $\gtrsim 2.3$   $\mu\text{m}$  because of the H<sub>2</sub>O and CO absorption bands, as seen in the spectrum plotted in Fig. 1b. Therefore, if the observed data are interpreted as due to a dust envelope, its flux contribution is higher at  $\lesssim 2.1$   $\mu\text{m}$  and  $\gtrsim 2.3$   $\mu\text{m}$ , resulting in a larger apparent size. In addition, the extended atmosphere makes the central star appear to be larger in the CO and H<sub>2</sub>O bands than at  $\sim 2.2$   $\mu\text{m}$ . This also leads to the observed increase in the angular size at  $\lesssim 2.1$  and  $\gtrsim 2.3$   $\mu\text{m}$ .

## 4. Dust shell modeling of the SED and GRAVITY visibilities

We collected (spectro)photometric data from the visible to the mid-infrared for modeling of the SED and GRAVITY visibilities: GAIA spectrum (Gaia Collaboration et al. 2016, 2023), 2MASS *JHK<sub>s</sub>* photometry (Cutri et al. 2003), Spitzer/IRS spectrum at 7–21  $\mu\text{m}$  (Lebzelter et al. 2006<sup>3</sup>), WISE photometry (Cutri et al. 2014), and AKARI photometry (Ishihara et al. 2010). The data were corrected for the interstellar extinction with  $E(B - V) = 0.04$  (Harris 1996) and  $R_V = A_V/E(B - V) = 3.1$  using the wavelength dependence from Cardelli et al. (1989). We obtained a bolometric flux of  $5.1 \times 10^{-12}$  W m<sup>-2</sup> by integrating the de-reddened SED, which corresponds to a bolometric luminosity of  $3200 L_\odot$  with the adopted distance of 4.5 kpc. Combined with an effective temperature ( $T_{\text{eff}}$ ) of 3200 K adopted for the modeling below, it results in a photospheric radius ( $R_{\text{ph}}$ ) of  $185 R_\odot$ . While 47 Tuc V3 is a variable star as mentioned in Sect. 2, the collected (spectro)photometric data were taken at widely different epochs. Lebzelter & Wood (2005) measured a *K*-band variability amplitude of  $\Delta K \approx 1$  mag, which affects the bolometric flux and thus the luminosity. Lebzelter et al. (2014) obtained  $T_{\text{eff}} = 3590$  K and  $L_\star = 4590 L_\odot$  for variability phase 0.18. We checked the effects of the variations in  $T_{\text{eff}}$  and  $L_\star$  on the dust shell modeling, as described below.

We carried out radiative transfer modeling with our Monte Carlo radiative transfer code *mcsim\_mpi* (Ohnaka et al. 2006). For the parameters of the central star and grain properties, we adopted those determined from the SED modeling of V3 by Mc11a. Those authors derived a value of  $T_{\text{eff}} = 3153$  K and a surface gravity of  $\log g = -0.25$ . The radiation from the

<sup>3</sup> Downloaded from the Spitzer Data Archive  
<https://irsa.ipac.caltech.edu/applications/Spitzer/SHA/>

<sup>2</sup> <https://www.eso.org/sci/software/pipelines/gravity/>

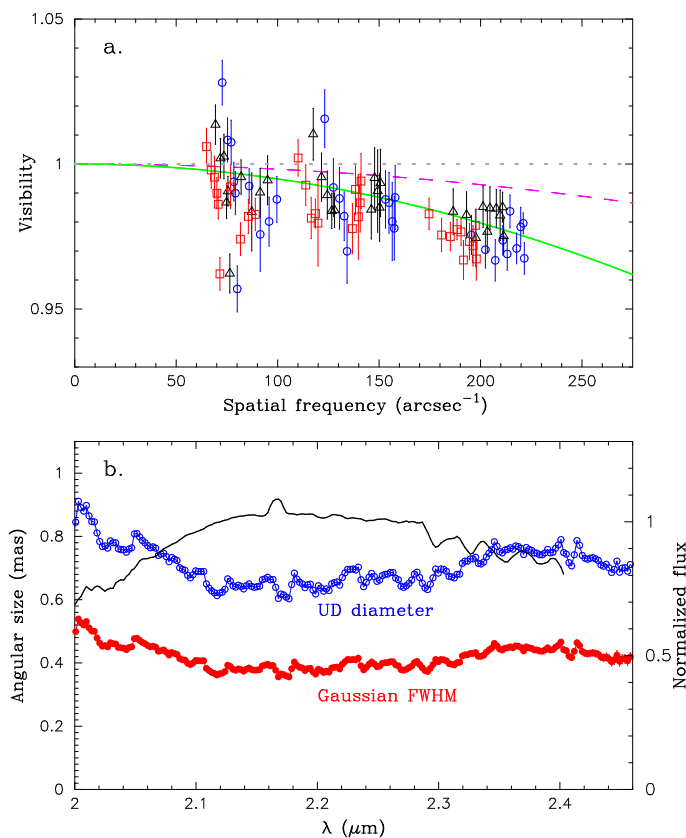


**Fig. 1.** GRAVITY observations of the AGB star V3 in the metal-poor globular cluster 47 Tuc. **a:** Visibilities observed at 2.1, 2.2, and 2.35 μm are plotted with the blue circles, black triangles, and red squares, respectively. The green solid line represents the visibility from the UD fit with an angular diameter of 0.65 mas derived at 2.2 μm, while the purple dashed line represents the uniform-disk visibility expected from the central star with a UD diameter of 0.38 mas. The gray horizontal dotted line marks the visibility 1. **b:** Wavelength dependence of the FWHM and angular diameter obtained by the Gaussian fit and UD fit to the observed visibilities are shown by the red filled circles and blue open circles, respectively. The black solid line shows the normalized spectrum derived from the GRAVITY data. The peak seen at ~2.165 μm is not real, but caused instead by the Br γ absorption line seen in the calibrator’s spectrum, which was not entirely removed by our spectroscopic calibration. The spectrum is cut off at ~2.4 μm because the spectrum of the proxy star used in the spectroscopic calibration only extends to 2.42 μm.

central star was approximated with the synthetic spectrum of the MARCS model (Gustafsson et al. 2008<sup>4</sup>) with parameters that are as close as possible to the above values of  $T_{\text{eff}}$  and  $\log g$ . We selected the MARCS model with  $T_{\text{eff}} = 3200$  K,  $\log g = 0.0$ ,  $M_{\star} = 1.0 M_{\odot}$ ,  $v_{\text{micro}}$  (micro-turbulent velocity) = 2.0 km s<sup>-1</sup>, along with the moderately CN-cycled chemical composition with  $[\text{Fe}/\text{H}] = -0.5$ . The synthetic spectrum was spectrally binned to match the spectral resolution of our GRAVITY data.

The SED modeling of metal-poor dusty stars in 47 Tuc reported by Mc11a shows that the primary dust component is metallic iron. In the case of V3, they concluded that the metallic iron fraction is 100% based on the absence of the spectral features due to silicate and corundum in the Spitzer/IRS spectrum (Lebzelter et al. 2006) and the ground-based spectrum (van

Loon et al. 2006). Therefore, we assumed metallic iron grains in our modeling and the opacity was calculated with the complex refractive index of Ordal et al. (1988). The grain size was assumed to be the standard Mathis, Rumpl, & Nordsieck (MRN) distribution (Mathis et al. 1977), with a minimum and maximum grain size of 0.005 and 0.25 μm, respectively. We adopted the power-law radial density profile, described as  $\rho \propto r^{-p}$ .

The free parameters of the dust shell are the optical depth at 0.55 μm ( $\tau_{0.55}$ ), the temperature at the inner boundary radius ( $T_{\text{in}}$ ) of the dust shell, and the power-law exponent,  $p$ , of the density profile. The outer radius of the dust shell was fixed to be 5000 times larger than the inner boundary radius, but the outer radius does not affect the results of our modeling. As described in Sect. 3, the extended atmosphere of V3 can make the central star’s apparent size larger than the photospheric angular diameter of 0.38 mas. To take this effect into account, the central star’s angular diameter was increased by a factor of  $f$  in the calculation of the model visibility. We treated  $f$  as a free parameter, adopting  $f = 1$  (no extended atmosphere), 1.35, and 1.7 (with the atmosphere’s angular diameter equal to the observed 2.2 μm UD diameter of 0.65 mas).

Figure 2 shows a comparison of the observed SED and visibilities with those predicted by one of the best-fitting models, with  $\tau_{0.55} = 0.15$ ,  $p = 2$ ,  $T_{\text{in}} = 700$  K (corresponding to an inner radius of 35  $R_{\text{ph}}$ ), and  $f = 1.35$ . The model visibilities plotted in Fig. 2b indicate that the visibility dips at spatial frequencies of  $\lesssim 60$  arcsec<sup>-1</sup> are attributed to the dust shell (i.e., it is resolved out at the baselines of our observations), while the visibilities at higher spatial frequencies are attributed to the extended atmosphere of the central star. The observed SED and the GRAVITY visibilities are reasonably fitted by the model, given the errors in the data. The model predicts the decrease in the visibilities at  $\lesssim 2.1$  and  $\gtrsim 2.3$  μm to be less pronounced than the observed data as seen in Figs. 2c, 2d, and 2g. This is because the wavelength dependence of the extended atmosphere is not included in our modeling. The slight dip at ~2.3 μm is due to the increase in the flux contribution of the dust shell, which makes the object’s overall size slightly larger (i.e., visibility lower).

Figure C.1 shows an alternative model, where the observed visibilities are mostly explained by the extended atmosphere with only a small contribution from the dust shell. This model is characterized by  $\tau_{0.55} = 0.1$ ,  $p = 2$ ,  $T_{\text{in}} = 500$  K, and  $f = 1.7$ . It should be noted that the inner boundary temperature is very low (corresponding to an inner radius of 90  $R_{\text{ph}}$ ) and, therefore, the flux contribution of the dust shell at 2–2.45 μm is  $\lesssim 0.5\%$ . The figure shows that the fit to the observed data is comparable to the model shown in Fig. 2. We found that the dust shell models with  $\tau_{0.55} = 0.1$ –0.25,  $T_{\text{in}} = 500$ –800 K, and  $p = 2$ –2.5 are able to aptly reproduce the data. Models with lower  $T_{\text{in}}$  have higher values of  $f$ , as, for instance, seen in the above two models.

If we adopt the higher  $T_{\text{eff}}$  and  $L_{\star}$  determined by Lebzelter et al. (2014), the fit to the GAIA data in the visible is very poor, because the 3500 K MARCS model predicts the TiO absorption to be much less shallow than observed. If we only fit the SED longward of ~1 μm and the GRAVITY visibilities, the best-fitting models have  $\tau_{0.55} = 0.05$ –0.15 and  $T_{\text{in}} = 500$ –800 K with  $p = 2$ –2.5. While the dust shell is slightly more optically thin, its inner boundary temperature is not significantly affected by the uncertainties in  $T_{\text{eff}}$  and  $L_{\star}$ .

Our modeling shows that the GRAVITY visibilities of V3 can be explained by the dust shell and/or the extended atmosphere of the central star. While the atmospheric extension,  $f$ , remains ambiguous between 1 and 1.7, the inner boundary temperature ranges from 500 to 800 K. These temperatures are no-

<sup>4</sup> <https://marcs.astro.uu.se/>

ticeably lower than the condensation temperature of  $\sim 1500$  K of corundum ( $\text{Al}_2\text{O}_3$ ) and Fe-free silicates such as forsterite ( $\text{Mg}_2\text{SiO}_4$ ) and enstatite ( $\text{MgSiO}_3$ ) found in nearby oxygen-rich AGB stars (Khouri et al. 2016; Ohnaka et al. 2016, 2017; Ohnaka & Adam 2019). Mc11a obtained an inner boundary temperature of 1000 K for V3 from their SED fitting (with 100% metallic iron as mentioned above) – lower than 1500 K but still higher than 500–800 K. The inner boundary temperatures of 500–800 K correspond to radii of 90–23  $R_{\text{ph}}$ , which is much larger than  $\sim 2$  stellar radii reported in the aforementioned studies of the nearby oxygen-rich AGB stars. The mid-infrared spectrum of V3 does not show a trace of the silicates or corundum in spite of their higher condensation temperatures compared to metallic iron. Mc11a pointed out that it is not clear how metallic iron condenses before the Mg-rich (and Fe-poor) silicates or corundum. This question becomes more serious, with the inner boundary temperature shown to be even lower based on our modeling of the GRAVITY data.

We calculated the ratio of the acceleration due to the radiation pressure on metallic iron grains to the gravity using:

$$\beta_{\text{dust}} = 1146 \frac{L_{\star}}{10^4 L_{\odot}} \frac{1}{M_{\star} (M_{\odot})} \frac{Q}{0.2} \frac{1}{a(\mu\text{m})} \frac{1}{\rho_{\text{bulk}} (\text{g cm}^{-3})} \frac{1}{r_{\text{gd}}},$$

where  $L_{\star}$ ,  $M_{\star}$ ,  $Q$ ,  $a$ ,  $\rho_{\text{bulk}}$ , and  $r_{\text{gd}}$  are the luminosity of the central star, its mass, the flux-mean opacity, the grain radius, the bulk density of dust grains, and the gas-to-dust ratio, respectively (Yamamura et al. 2000). We calculated the flux-mean opacity of metallic iron dust with the stellar spectrum used in our modeling for different grain sizes of 0.005, 0.1, and 0.25  $\mu\text{m}$ . Assuming a gas-to-dust ratio of 1000 (Mc11a),  $\rho_{\text{bulk}} = 7 \text{ g cm}^{-3}$ , and a stellar mass of 0.6–0.7  $M_{\odot}$  (McDonald et al. 2011b; Lebzelter et al. 2014), the ratio is 0.55, 2.5, and 3.7 for the grain size of 0.005, 0.1, and 0.25  $\mu\text{m}$ , respectively, with a ratio of 1 reached for a grain size of  $\sim 0.05 \mu\text{m}$ . This means that grains smaller than  $\sim 0.05 \mu\text{m}$  are not blown away by the radiation pressure.

On the other hand, Mc11a suggested that metallic iron grains in the stars in 47 Tuc are small or elongated and/or they condense more efficiently than at the solar metallicity, to account for the mass-loss rate and the wind terminal velocity. As an example, they presented a case with iron grains five times smaller than the standard MRN size distribution, which means that the maximum grain size is 0.05  $\mu\text{m}$ . However, they noted that both effects – the smaller iron grain size and elongated grains – are relevant and, therefore, they could not specify the size of the small grains; it seems likely that the size is in the aforementioned range, where the radiation pressure on iron grains does not lead to mass loss. This implies, as Mc11a concluded, that the mass loss in V3 as well as other cool evolved stars in 47 Tuc may not be driven by radiation pressure on dust grains, but by some other mechanism(s) instead. In this case, dust formation is a mere result – and not the source – of the mass loss.

## 5. Conclusion

Our VLTI/GRAVITY observations have spatially resolved, for the first time, an individual star, V3, in the metal-poor globular cluster 47 Tuc at 2–2.45  $\mu\text{m}$ . The observed GRAVITY data translate into a Gaussian FWHM angular size of  $\sim 0.4$  mas and a UD diameter of  $\sim 0.7$  mas. Our radiative transfer modeling suggests that the observed SED and GRAVITY data can be explained by an optically thin dust shell with  $\tau_{0.55} = 0.05\text{--}0.25$ , consisting of metallic iron grains, likely with effects of the extended atmosphere of the central star. The dust condensation temperature was

found to be 500–800 K, significantly lower than found in nearby Galactic AGB stars.

GRAVITY observations at shorter and longer baselines than those seen in the present data are necessary to better constrain the properties of the dust shell and the extended atmosphere of the central star, respectively. To further study the formation of metallic iron grains, thermal-infrared interferometric observations will be useful. The VLTI/MATISSE instrument allows us to spatially resolve V3 simultaneously at 3–4.2  $\mu\text{m}$ , 4.5–5  $\mu\text{m}$ , and 8–13  $\mu\text{m}$ . In particular, observations in the 10  $\mu\text{m}$  region are important for examining whether there is a trace of grain species other than metallic iron in the spatially resolved data.

*Acknowledgements.* We thank the ESO Paranal team for supporting our VLTI observations. K.O. acknowledges the support of the Agencia Nacional de Investigación Científica y Desarrollo (ANID) through the FONDECYT Regular grant 1210652. This research made use of the SIMBAD database, operated at the CDS, Strasbourg, France. This publication makes use of data products from the Two Micron All Sky Survey, which is a joint project of the University of Massachusetts and the Infrared Processing and Analysis Center/California Institute of Technology, funded by the National Aeronautics and Space Administration and the National Science Foundation. This publication makes use of data products from the Wide-field Infrared Survey Explorer, which is a joint project of the University of California, Los Angeles, and the Jet Propulsion Laboratory/California Institute of Technology, funded by the National Aeronautics and Space Administration. This research has made use of the NASA/IPAC Infrared Science Archive, which is funded by the National Aeronautics and Space Administration and operated by the California Institute of Technology. This research is based on observations with AKARI, a JAXA project with the participation of ESA. This work has made use of data from the European Space Agency (ESA) mission *Gaia* (<https://www.cosmos.esa.int/gaia>), processed by the *Gaia* Data Processing and Analysis Consortium (DPAC, <https://www.cosmos.esa.int/web/gaia/dpac/consortium>). Funding for the DPAC has been provided by national institutions, in particular the institutions participating in the *Gaia* Multilateral Agreement.

## References

- Adam, C., & Ohnaka, K. 2019, *A&A*, 628, A132  
 Bourges, L., Mella, G., Lafrasse, S., et al. 2017, *JMMC Stellar Diameters Catalogue Version 2*  
 Boyer, M. L., McDonald, I., van Loon, J. Th., et al. 2009, *ApJ*, 705, 746  
 Cardelli, J. A., Clayton, G. C., & Mathis, J. S. 1989, *ApJ*, 345, 245  
 Cutri R. M., Skrutskie M. F., Van Dyk S., et al. 2003, *The 2MASS All-Sky Catalog of Point Sources*  
 Cutri, R. M., Wright, E. L., Conrow, T., et al. 2014, *AllWISE Data Release (2013)*  
 Gaia Collaboration, Prusti, T., de Bruijne, J. H. J., et al. 2016b, *A&A*, 595, A1  
 Gaia Collaboration, Vallenari, A., Brown, A. G. A., et al. 2023, *A&A*, 674, A1  
 Goldman, S. R., van Loon, J. Th., Zijlstra, A. A., et al. 2017, *MNRAS*, 465, 403  
 GRAVITY Collaboration, Abuter, R., Accardo, M., et al. 2017, *A&A*, 602, A94  
 Gustafsson B., Edvardsson B., Eriksson K., et al. 2008, *A&A*, 486, 951  
 Harris, W. E., 1996 *ApJ*, 112, 1487  
 Ishihara, D., Onaka, T., Kataza, H., et al. 2010, *A&A*, 514, A1  
 Khouri, T., Maercker, M., Waters, L. B. F. M., et al. 2016, *A&A*, 591, A70  
 Lebzelter, T., & Wood, P. R. 2005, *A&A*, 441, 1117  
 Lebzelter, T., Wood, P. R., Hinkle, K. H., Joyce, R. R., Fekel, F. C. 2005, *A&A*, 432, 207  
 Lebzelter, Th., Posch, Th., Hinkle, K., Wood, P. R., & Bouwman, J. 2006, *ApJL*, 653, 145  
 Lebzelter, T., Nowotny, W., Hinkle, K. H., Höfner, S., & Aringer, B. 2014, *A&A* 567, A143  
 Mathis, J. S., Rumpl, W., & Nordsieck, K. H. 1977, *ApJ*, 217, 425  
 McDonald, I., Boyer, M. L., van Loon, J. Th., & Zijlstra, A. A. 2011a, *ApJ*, 730, 71 (Mc11a)  
 McDonald, I., Boyer, M. L., van Loon, J. Th., et al. 2011b, *ApJS*, 193, 23  
 McDonald, I., Boyer, M. L., Groenewegen, M. A. T., et al. 2019, *MNRAS*, 484, L85  
 Ohnaka, K., Driebe, T., Hofmann, K.-H., et al. 2006, *A&A*, 445, 1015  
 Ohnaka, K., Weigelt, G., & Hofmann, K.-H. 2016, *A&A*, 589, A91  
 Ohnaka, K., Weigelt, G., & Hofmann, K.-H. 2017, *A&A*, 597, A20  
 Ordal, M. A., Bell, R. J., Alexander, R. W., Newquist, L. A., & Query, M. R. 1988, *Appl. Opt.*, 27, 1203  
 Rayner, J. T., Cushing, M. C., & Vacca, W. D. 2009, *ApJS*, 185, 289

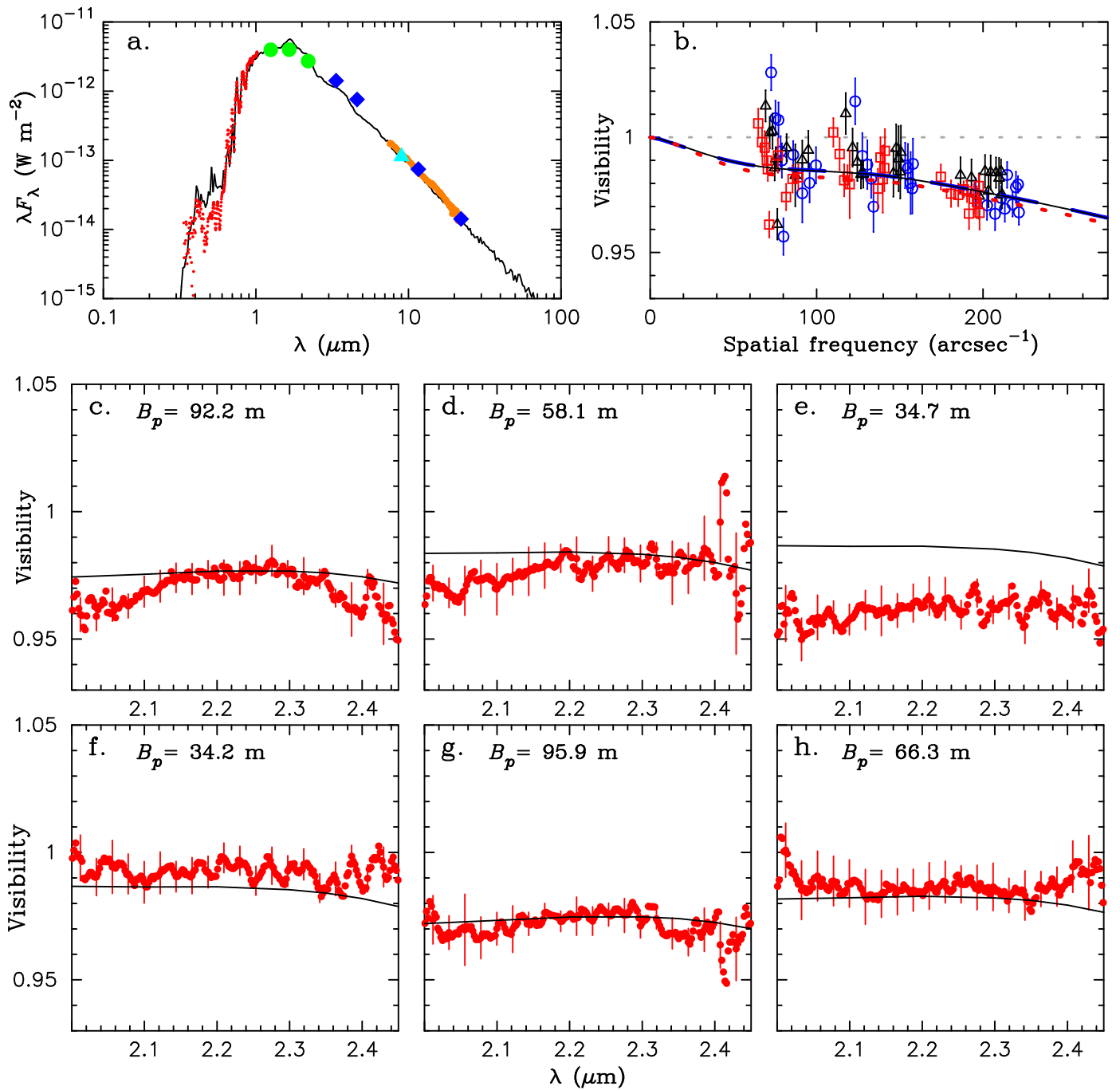


**Fig. 2.** Dust shell modeling of the SED and GRAVITY visibilities of 47 Tuc V3. **a:** Comparison of the observed and model SEDs. The solid line represents the best-fitting model with  $\tau_{0.55} = 0.15$  and an inner boundary temperature of 700 K. The red dots, green circles, blue diamonds, light blue triangle, and thick orange line represent the GAIA spectrum, 2MASS  $JHK_s$  photometric data, WISE photometric data, AKARI data, and Spitzer/IRS spectrum, respectively. **b:** Comparison of the observed and model visibilities as a function of spatial frequency. The blue circles, black triangles, and red squares correspond to the visibilities measured at 2.1, 2.2, and 2.35  $\mu$ m, respectively. The blue long-dashed line, black solid line (almost entirely overlapping with the long-dashed line), and red dotted line represent the model visibilities predicted at 2.1, 2.2, and 2.35  $\mu$ m, respectively. The gray horizontal dotted line marks the visibility 1. **c–h:** Comparison of the visibilities as a function of wavelength. In each panel, the red dots represent the observed data, while the black line represents the model.

- van Loon, J. Th., Cioni, M.-R. L., Zijlstra, A. A., & Loup, C. 2005, A&A, 438, 273  
 van Loon, J. Th., McDonald, I., Oliveira, J. M., et al. 2006, A&A 450, 339  
 Vassiliadis, E., & Wood, P. R 1993, ApJ, 413, 641  
 Wittkowski, M., Boboltz, D. A., Driebe, T., et al. 2008, A&A, 479, L21  
 Woodruff, H. C., Tuthill, P. G., Monnier, J. D., et al. 2008, ApJ, 673, 418  
 Woodruff, H. C., Ireland, M. J., Tuthill, P. G., et al. 2009, ApJ, 691, 1328  
 Yamamura, I., Dominik, C., de Jong, T., Waters, L. B. F. M., & Molster, F. J. 2000, A&A, 363, 629

**Table A.1.** Summary of our VLTI/GRAVITY observations of 47 Tuc V3.

#	$t_{\text{obs}}$ UTC	$B_p$ (m)	PA ( $^\circ$ )	Seeing ( $''$ )	$\tau_0$ (ms)
2023 October 14					
AT configuration: D0-G2-K0-J3					
47 Tuc V3					
DIT = 10 s, $N_f = 32$ , $N_{\text{exp}} = 2$					
1	00:29:47	92.2/58.1/34.7/ 34.3/95.9/66.3	13/15/-72/ 10/34/47	0.65	6.6
2	01:16:17	91.3/57.5/37.2/ 33.9/95.6/67.0	22/25/-63/ 19/45/58	0.44	10.5
3	02:05:59	89.7/56.5/39.6/ 33.4/95.1/67.7	32/35/-53/ 28/57/70	0.62	5.6
4	02:52:47	87.6/55.2/41.4/ 32.6/94.2/68.1	42/44/-44/ 37/68/82	0.55	4.4
5	03:44:14	84.6/53.3/43.1/ 31.5/92.8/68.3	52/55/-35/ 47/80/-86	0.44	5.3
Calibrator HD3689					
DIT = 10 s, $N_f = 32$ , $N_{\text{exp}} = 2$					
C1	00:04:50	91.0/57.4/32.1/ 33.7/95.9/66.1	6/8/97/ 2/25/37	0.65	7.2
C2	00:53:08	90.4/57.0/34.8/ 33.5/95.7/66.8	15/18/-72/ 12/37/49	0.57	7.5
C3	01:40:08	89.4/56.4/37.1/ 33.1/95.3/67.4	25/27/-63/ 21/48/61	0.53	12.0

**Notes.**  $B_p$ : Projected baseline length. PA: Position angle of the baseline vector projected onto the sky. DIT: Detector Integration Time.  $N_f$ : Number of frames in each exposure.  $N_{\text{exp}}$ : Number of exposures. The seeing and the coherence time ( $\tau_0$ ) were measured in the visible band.

## Appendix A: Observation log

Table A.1 shows the summary of our GRAVITY observations of 47 Tuc V3 and the calibrator HD3689.

## Appendix B: Spectroscopic calibration of the GRAVITY spectrum

The spectroscopic calibration to remove the telluric lines and instrumental effects was carried out as:

$$F_{\text{sci}}^{\text{true}} = F_{\text{sci}}^{\text{obs}} \times F_{\text{cal}}^{\text{true}} / F_{\text{cal}}^{\text{obs}},$$

where  $F_{\text{sci}(\text{cal})}^{\text{true}}$  and  $F_{\text{sci}(\text{cal})}^{\text{obs}}$  denote the true and observed spectra of the science target (sci) or the calibrator (cal) HD3689, respectively. To approximate the true spectrum of HD3689 (F6V), we used the spectrum of  $\xi$  Peg taken with the InfraRed Telescope Facility (IRTF Spectral Library<sup>5</sup>, Rayner et al. 2009) because its spectral type and luminosity class F6V is the same as that of HD3689. The IRTF spectrum taken with a spectral resolution of  $\lambda/\Delta\lambda = 2000$  was convolved to match the spectral resolution of 200 of our GRAVITY data and then used for  $F_{\text{cal}}^{\text{true}}$  in the above spectroscopic calibration. The calibrated spectrum of 47 Tuc V3 was normalized with the flux at  $2.2 \mu\text{m}$ , where the flux is the least affected by the H<sub>2</sub>O and CO bands.

## Appendix C: Alternative model with little contribution of the dust shell

Figure C.1 shows a comparison of the observed SED and GRAVITY visibilities with a model where the flux contribution of the

<sup>5</sup> [http://irtfweb.ifa.hawaii.edu/~spex/IRTF\\_Spectral\\_Library/](http://irtfweb.ifa.hawaii.edu/~spex/IRTF_Spectral_Library/)

dust shell at  $2\text{--}2.45 \mu\text{m}$  is smaller than  $\sim 0.5\%$ . In this case, the visibilities observed at  $2\text{--}2.45 \mu\text{m}$  are accounted for by the atmosphere of the central star extending to  $1.7 R_{\text{ph}}$ .

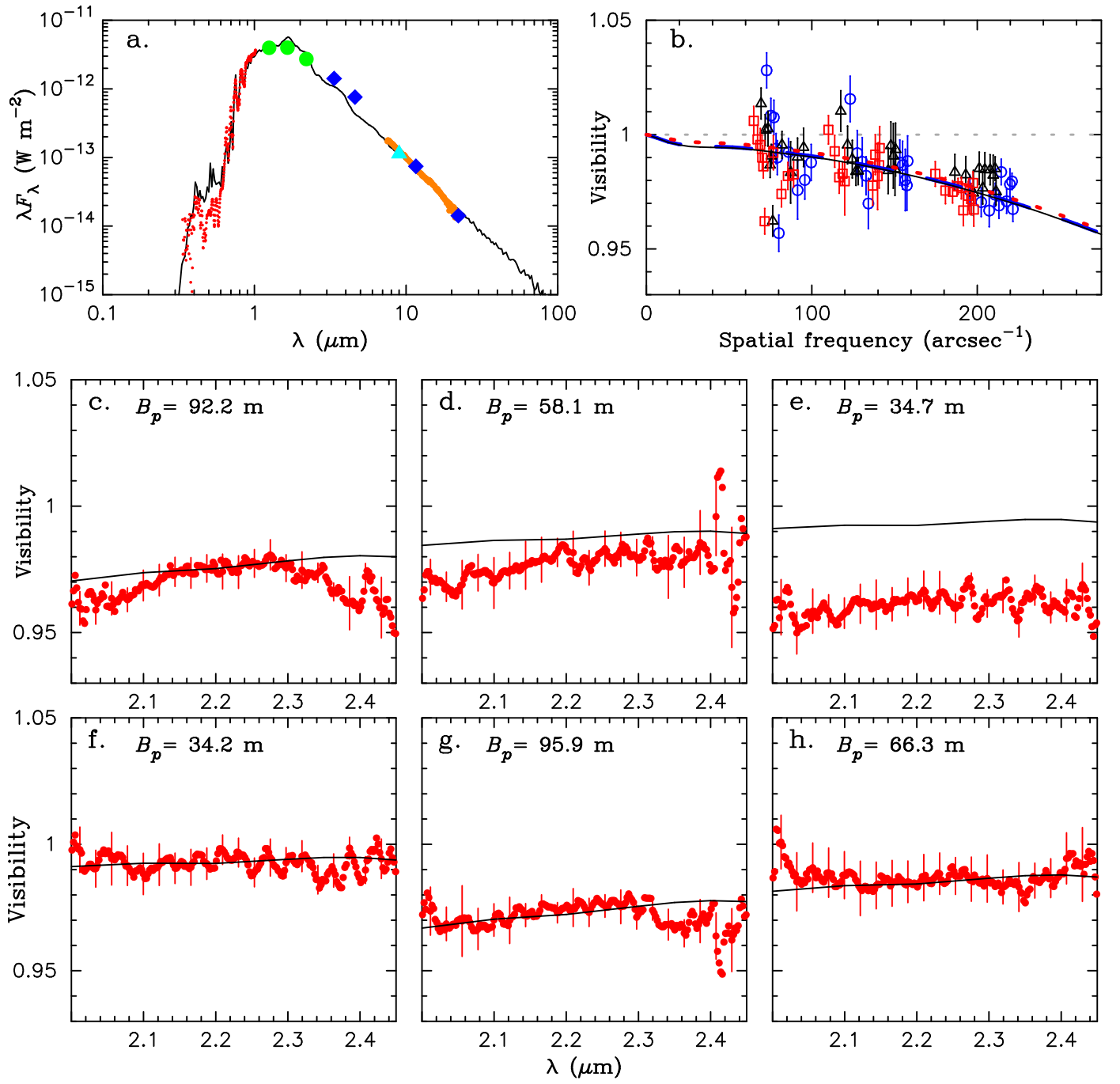


**Fig. C.1.** Alternative model for the SED and GRAVITY visibilities of 47 Tuc V3 with little flux contribution from the dust shell, shown in the same manner as in Fig. 2.